Refining the detection of the zero crossing for the three-gluon vertex in symmetric and asymmetric momentum subtraction schemes

Ph. Boucaud,[1] F. De Soto,[2] J. Rodríguez-Quintero,[3,4] and S. Zafeiropoulos[5,6]

[1]*Laboratoire de Physique Théorique (UMR8627), Cnetre Nationale de la Recherche Scientifique,
Université de Paris-Sud, Université Paris-Saclay, 91405 Orsay, France*
[2]*Departamento de Sistemas Físicos, Químicos y Naturales, Universidad Pablo de Olavide,
41013 Sevilla, Spain*
[3]*Department of Integrated Sciences; University of Huelva, E-21071 Huelva, Spain*
[4]*CAFPE, Universidad de Granada, E-18071 Granada, Spain*
[5]*Department of Physics, College of William and Mary, Williamsburg, Virginia 23187-8795, USA*
[6]*Jefferson Laboratory, 12000 Jefferson Avenue, Newport News, Virginia 23606, USA*

This article reports on the detailed study of the three-gluon vertex in four-dimensional $SU(3)$ Yang-Mills theory employing lattice simulations with large physical volumes and high statistics. A meticulous scrutiny of the so-called symmetric and asymmetric kinematical configurations is performed, and it is shown that the associated form factor changes sign at a given range of momenta. The lattice results are compared to the model-independent predictions of Schwinger-Dyson equations, and a very good agreement between the two is found.

I. INTRODUCTION

The theory describing the strong interactions, QCD, is essentially a quantum field theory based on a local non-Abelian gauge theory which, in its IR sector, possesses a very rich and intricate structure controlling its low-momentum dynamics. Phenomena such as confinement and chiral symmetry breaking, and hence the origin of most of the baryonic mass, are clearly rooted in the IR sector of the theory. The understanding of this IR dynamics is crucial, and, indeed, it has been very much boosted in the last few years, mainly due to very careful and detailed studies of the fundamental Green's functions of the theory in both lattice [1–8] and continuum QCD [9–30]. It is not worthless to remind the reader here that those fundamental Green's functions are essential building blocks in the construction of any proper symmetry-preserving truncation of Schwinger-Dyson equations (SDEs) in order to define a tractable continuum bound-state problem able to reproduce the observable properties of hadrons [14,31–38].

The endeavors in obtaining a two-point Green's function from large-volume lattice simulations [4–8] crystallized in our current well-known picture about the infrared finiteness of both the gluon propagator and ghost dressing function. This picture has been consistently interpreted by using a variety of approaches, such as the so-called refined Gribov-Zwanziger scenario [22,23], effective descriptions based on the Curci-Ferrari model [39,40] or SDEs under different truncation schemes [9–13]. In particular, one of the approaches within this last class [9] is based on the combination of the pinch technique (PT) and the background field method (BFM). This latter PT-BFM framework [41] allows for a systematical rearranging of classes of diagrams in the nonperturbative expansion for the SDEs, leading to modified Green's functions obeying linear (Abelian-like) Slavnov-Taylor identities (STIs). A subtle realization of the Schwinger mechanism, within this framework, takes place and endows the gluon with an effective—dynamically acquired—mass [42–45]. Furthermore, a profound connection emerges between the massless nature of the ghost propagator, the very deep IR behavior of the gluon, and zero-momentum divergences of the three-gluon vertex that should be observed in some particular kinematic limits [46]. The latter is valid in the Landau gauge in three as well as four dimensions. The entanglement of these features stems precisely from how the mass-generation mechanism remains transparent for the ghosts which, contrarily to the gluons, appear to flow in the quantum loops without the IR *protection* of a running mass. As a consequence of this, some of the form factors of the nonperturbative three-gluon vertex appear to be dominated in the IR by the non-perturbative ghost-loop contribution, taking negative values and diverging at vanishing momentum, precisely as a logarithm in four dimensions [46]. Hence, they change sign at a zero crossing which takes place in the IR.

The same IR pattern has also been claimed by independent SDE analysis, employing various approaches and truncation schemes, in the three-gluon [40,46–50] and four-gluon [51,52] sectors, although the zero crossing is predicted to happen at such a low momentum that it is difficult to be revealed by realistic lattice QCD simulations. Some studies in an $SU(2)$ lattice gauge theory showed this expected pattern for the three-gluon vertex to emerge in three dimensions but failed to be conclusive in four [1,2], and, very

recently, two independent investigations [53,54] in $SU(3)$ have provided a preliminary confirmation for this to happen for the three-gluon vertex also in four dimensions.

In this article, we aim for the completion of the preliminary work presented in Ref. [53] by largely increasing the statistics—the number of gauge-field configurations as well as the number of different lattice setups—and by performing a more elaborated and refined analysis, based on the SDE interpretation of the IR three-gluon behavior, intended for a better detection of the zero crossing and to solidify our theoretical understanding of its happening. To this purpose, we have performed $SU(3)$ simulations in large four-dimensional volumes with two lattice actions (Wilson plaquette and tree-level Symanzik), computed the three-gluon Green's function, and projected out the relevant form factor in two different kinematical configurations. We introduced all the definitions and carefully described the procedure for the extraction of the form factors from the nonperturbative lattice Green's functions, the renormalization scheme, and the connection with the running strong coupling in Sec. II. Section III is devoted to providing the details of the simulations, the lattice actions, and setups and to displaying the results for the running strong coupling and the form factors. The analysis of the lattice results can be found in Sec. IV, where we also discuss their interpretation, and, finally, we conclude in Sec. V.

II. THREE-GLUON GREEN'S FUNCTION AND THE RUNNING COUPLING

A. Definitions of the connected and 1-PI vertex functions

Let us first define the connected three-gluon vertex as the correlation function of the following gauge fields, $\tilde{A}$, taken in Fourier space at the three-momenta p, q, and r, such that $p + q + r = 0$,

$$
\mathcal{G}_{\alpha\mu\nu}^{abc}(p,q,r) = \langle \tilde{A}_{\mu}^{a}(p)\tilde{A}_{\nu}^{b}(q)\tilde{A}_{\rho}^{c}(q)\rangle
$$
$$
= f^{abc}\mathcal{G}_{\alpha\mu\nu}(p,q,r), \qquad (2.1)
$$

where the sub- (super-)indices are Lorentz (color) ones and the average $\langle\cdot\rangle$ indicates functional integration over the gauge space. For the sake of convenience, we will work in the Landau gauge, in which only the projection onto the totally antisymmetric color tensor, f^{abc}, survives for the three-gluon Green's function, making Eq. (2.1) plainly general. In terms of the usual one-particle irreducible (1-PI) vertex function, Γ, and the gluon propagator

$$
\Delta_{\mu\nu}^{ab}(p) = \langle \tilde{A}_{\mu}^{a}(p)\tilde{A}_{\nu}^{b}(-p)\rangle = \Delta(p^2)\delta^{ab}P_{\mu\nu}(p), \quad (2.2)
$$

with $P_{\mu\nu}(p) = \delta_{\mu\nu} - p_{\mu}p_{\nu}/p^2$, the three-gluon Green's function can be recast as

$$
\mathcal{G}_{\alpha\mu\nu}^{abc}(p,q,r) = gf^{a'b'c'}\Gamma_{\alpha'\mu'\nu'}(p,q,r)\Delta_{\alpha'\alpha}^{a'a}(p)\Delta_{\mu'\mu}^{b'b}(q)\Delta_{\nu'\nu}^{c'c}(r)
$$
$$
(2.3)
$$

$$
= gf^{abc}\Gamma_{\alpha'\mu'\nu'}(p,q,r)\Delta(p^2)\Delta(q^2)\Delta(r^2)
$$
$$
\times P_{\alpha'\alpha}(p)P_{\mu'\mu}(q)P_{\nu'\nu}(r), \qquad (2.4)
$$

where g is the strong coupling constant. Thus, the vertex function $\mathcal{G}_{\alpha\mu\nu}$, introduced in Eq. (2.1), can be easily seen in Eq. (2.4) to read in terms of gluon dressing functions and transversal projectors such that the transversality condition

$$
p_{\alpha}\mathcal{G}_{\alpha\mu\nu}(p,q,r) = q_{\mu}\mathcal{G}_{\alpha\mu\nu}(p,q,r) = r_{\nu}\mathcal{G}_{\alpha\mu\nu}(p,q,r) = 0
$$
$$
(2.5)
$$

is made clearly apparent. A basis of four tensors can generally describe the subspace where the vertex function $\mathcal{G}_{\alpha\mu\nu}$ is embedded [46,49,55]. However, in what follows, we will specialize in two particular momenta configurations for the three-gluon vertex which, from now on, will be called *symmetric* and *asymmetric*. The first one corresponds to the case defined by $p^2 = q^2 = r^2$ and $p \cdot q = p \cdot r = q \cdot r = -p^2/2$, in which the subspace of the totally transverse tensors, observing Eq. (2.5), has dimension 2. Hence, a basis is made by only two tensors, namely

$$
\lambda_{\alpha\mu\nu}^{\text{tree}}(p,q,r) = \Gamma_{\alpha'\mu'\nu'}^{(0)}(p,q,r)P_{\alpha'\alpha}(p)P_{\mu'\mu}(q)P_{\nu'\nu}(r),
$$
$$
\lambda_{\alpha\mu\nu}^{\text{S}}(p,q,r) = \frac{(p-q)_{\nu}(q-r)_{\alpha}(r-p)_{\mu}}{p^2}, \qquad (2.6)
$$

where $\Gamma_{\alpha\mu\nu}^{(0)}(p,q,r) = \delta_{\alpha\mu}(p-q)_{\nu} + \delta_{\mu\nu}(q-r)_{\alpha} + \delta_{\nu\alpha}(r-p)_{\mu}$ stands for the perturbative tree-level tensor of the three-gluon vertex, and one can write

$$
\mathcal{G}_{\alpha\mu\nu}(p,q,r) = T^{\text{sym}}(p^2)\lambda_{\alpha\mu\nu}^{\text{tree}}(p,q,r)
$$
$$
+ S^{\text{sym}}(p^2)\lambda_{\alpha\mu\nu}^{\text{S}}(p,q,r). \qquad (2.7)
$$

Now, taking advantage of the fact that the transverse projector acts over the subspace defined by the basis (2.6) as the identity,

$$
\lambda_{\alpha'\mu'\nu'}^{\text{tree}}(p,q,r)P_{\alpha'\alpha}(p)P_{\mu'\mu}(q)P_{\nu'\nu}(r) = \lambda_{\alpha\mu\nu}^{\text{tree}}(p,q,r)
$$
$$
\lambda_{\alpha'\mu'\nu'}^{\text{S}}(p,q,r)P_{\alpha'\alpha}(p)P_{\mu'\mu}(q)P_{\nu'\nu}(r) = \lambda_{\alpha\mu\nu}^{\text{S}}(p,q,r), \qquad (2.8)
$$

Eq. (2.7) can be rewritten as

$$
\mathcal{G}_{\alpha\mu\nu}(p,q,r) = (T^{\text{sym}}(p^2)\lambda_{\alpha'\mu'\nu'}^{\text{tree}}(p,q,r)
$$
$$
+ S^{\text{sym}}(p^2)\lambda_{\alpha'\mu'\nu'}^{\text{S}}(p,q,r))
$$
$$
\times P_{\alpha'\alpha}(p)P_{\mu'\mu}(q)P_{\nu'\nu}(r), \qquad (2.9)
$$

which, compared to Eq. (2.4), leads to the following decomposition for the transverse 1-PI vertex function:

$$g\Gamma_{\alpha\mu\nu}(p,q,r) = \frac{T^{\text{sym}}(p^2)}{\Delta^3(p^2)}\lambda^{\text{tree}}_{\alpha\mu\nu}(p,q,r)$$
$$+ \frac{S^{\text{sym}}(p^2)}{\Delta^3(p^2)}\lambda^{\text{S}}_{\alpha\mu\nu}(p,q,r) \qquad (2.10)$$

$$= g\Gamma^{\text{sym}}_T(p^2)\lambda^{\text{tree}}_{\alpha\mu\nu}(p,q,r)$$
$$+ g\Gamma^{\text{sym}}_S(p^2)\lambda^{\text{S}}_{\alpha\mu\nu}(p,q,r). \qquad (2.11)$$

Thus, focusing on the form factor for the tree-level tensor, we get

$$T^{\text{sym}}(p^2) = g\Gamma^{\text{sym}}_T(p^2)\Delta^3(p^2), \qquad (2.12)$$

where, in particular, the $T^{\text{sym}}(p^2)$ form factor can be projected out through

$$T^{\text{sym}}(p^2) = \frac{\mathcal{G}_{\alpha\mu\nu}(p,q,r)\mathcal{W}_{\alpha\mu\nu}(p,q,r)}{\mathcal{W}_{\alpha\mu\nu}(p,q,r)\mathcal{W}_{\alpha\mu\nu}(p,q,r)} \qquad (2.13)$$

with

$$\mathcal{W}_{\alpha\mu\nu}(p,q,r) = \lambda^{\text{tree}}_{\alpha\mu\nu}(p,q,r) + \frac{1}{2}\lambda^{\text{S}}_{\alpha\mu\nu}(p,q,r). \qquad (2.14)$$

The second special momenta configuration that we will focus our attention on is the so-called asymmetric one and is defined by taking the $p \to 0$ limit, while keeping at the same time the condition $q^2 = r^2 = -q \cdot r$. In this case, in the Landau gauge, only one transverse tensor can be constructed, and it appears to be the $p \to 0$ limit of the tree-level one,

$$\lambda^{\text{tree}}_{\alpha\mu\nu}(0,q,-q) = \Gamma^{(0)}_{\alpha\mu'\nu'}(0,q,-q)P_{\mu'\mu}(q)P_{\nu'\nu}(q)$$
$$= 2q_\alpha P_{\mu\nu}(q). \qquad (2.15)$$

It is straightforward to notice that the second tensor in Eq. (2.6), $\lambda^{\text{S}}_{\alpha\mu\nu}$, is only transverse if the symmetric condition $p^2 = q^2 = r^2$ is met. This is clearly not the case when the asymmetric configuration of momenta is considered, and, indeed, the $p \to 0$ limit of this second tensor would result in a totally longitudinal structure, $\lambda^{\text{S}}_{\alpha\mu\nu} \sim q_\alpha q_\mu q_\nu$.

Thus, we are left with a single form factor that can be projected out through

$$T^{\text{asym}}(q^2) = \frac{\mathcal{G}_{\alpha\mu\nu}(0,q,-q)\tilde{\mathcal{W}}_{\alpha\mu\nu}(0,q,-q)}{\tilde{\mathcal{W}}_{\alpha\mu\nu}(0,q,-q)\tilde{\mathcal{W}}_{\alpha\mu\nu}(0,q,-q)}, \qquad (2.16)$$

where now

$$\tilde{\mathcal{W}}_{\alpha\mu\nu}(0,q,-q) = \lambda^{\text{tree}}_{\alpha\mu\nu}(0,q,-q). \qquad (2.17)$$

This form factor relates to the 1-PI vertex function as follows,

$$T^{\text{asym}}(q^2) = g\Gamma^{\text{asym}}_T(q^2)\Delta(0)\Delta^2(q^2), \qquad (2.18)$$

where the $p \to 0$ limit brings here a dressing function evaluated at vanishing momentum that, as will be seen below, appears to be the source of additional statistical noise in extracting a nonperturbative signal for the form factor *via* Eq. (2.16) from lattice QCD.

B. *R*-projector

Aiming for a direct comparison with the lattice estimates for the three-gluon vertex given in Refs. [1,2], the authors of Ref. [46] define a particular quantity projected out through the so-called *R*-projector (constructed with the tree-level tensor, $\Gamma^{(0)}$),

$$R(p^2) = \frac{g\Gamma^{(0)}_{\alpha\mu\nu}(p,q,r)\mathcal{G}_{\alpha\mu\nu}(p,q,r)}{g\Gamma^{(0)}_{\alpha\mu\nu}(p,q,r)P^{\alpha\alpha'}(p)\Delta(p^2)P^{\mu\mu'}(q)\Delta(q^2)\Delta(r^2)P^{\nu\nu'}(r)g\Gamma^{(0)}_{\alpha'\mu'\nu'}(p,q,r)} \qquad (2.19)$$

$$= \frac{\Gamma^{(0)}_{\alpha\mu\nu}(p,q,r)P^{\alpha\alpha'}(p)P^{\mu\mu'}(q)P^{\nu\nu'}(r)\Gamma_{\alpha'\mu'\nu'}(p,q,r)}{\Gamma^{(0)}_{\alpha\mu\nu}(p,q,r)P^{\alpha\alpha'}(p)P^{\mu\mu'}(q)P^{\nu\nu'}(r)\Gamma^{(0)}_{\alpha'\mu'\nu'}(p,q,r)}, \qquad (2.20)$$

where Eq. (2.19) corresponds to the quantity evaluated in Ref. [1,2] from lattice QCD (see Eq. (20) of Ref. [1]), adapted to our notation here, which is rewritten in Ref. [46] as it reads in Eq. (2.20), in terms of the full nonperturbative vertex functions, $\Gamma_{\alpha\mu\nu}$, although

explicitly brought to transversity by the appropriate projectors.

Now, for the sake of completion, we will apply Eqs. (2.6) and (2.11) in Eq. (2.20) and then, for the symmetric momenta configuration, get

$$R(p^2) = \frac{\lambda^{\text{tree}\,\alpha\mu\nu}(p,q,r)[\Gamma_T^{\text{sym}}(p^2)\lambda_{\alpha\mu\nu}^{\text{tree}}(p,q,r) + \Gamma_S^{\text{sym}}(p^2)\lambda_{\alpha\mu\nu}^{S}(p,q,r)]}{\lambda^{\text{tree}\,\alpha\mu\nu}(p,q,r)\lambda_{\alpha\mu\nu}^{\text{tree}}(p,q,r)}$$

$$= \Gamma_T^{\text{sym}}(p^2) - \frac{6}{11}\Gamma_S^{\text{sym}}(p^2), \tag{2.21}$$

which shows that the R-projector applied to the three-gluon Green's function results in a combination of the two form factors for the tensors in Eq. (2.6), which form a basis for the dimension-2 transverse subspace in the symmetric case.

On the other hand, in the case of the asymmetric configuration of momenta, as the transverse subspace is only of dimension 1, the action of the R-projector,

$$\tilde{R}(q^2) = \frac{\Gamma_{\alpha\mu\nu}^{(0)}(0,q,-q)P^{\mu\mu'}(q)P^{\nu\nu'}(q)\Gamma_{\alpha\mu'\nu'}(0,q,-q)}{\Gamma_{\alpha\mu\nu}^{(0)}(0,q,-q)P^{\mu\mu'}(q)P^{\nu\nu'}(q)\Gamma_{\alpha\mu'\nu'}^{(0)}(0,q,-q)}$$

$$= \Gamma_T^{\text{asym}}(q^2), \tag{2.22}$$

is equivalent to Eq. (2.16).

C. Renormalization and the running coupling

All the quantities that have been introduced so far are bare, and one should everywhere understand an implicit dependence on the regularization cutoff. We apply now a given renormalization procedure where any renormalized Green's functions ought to be understood as the correlation function of renormalized gauge fields, $\tilde{A}_R = Z_3^{-1/2}\tilde{A}$, such that

$$\Delta_R(p^2;\mu^2) = Z_3^{-1}(\mu^2)\Delta(p^2), \tag{2.23}$$

$$T_R(p^2;\mu^2) = Z_3^{-3/2}(\mu^2)T(p^2), \tag{2.24}$$

where Eq. (2.24) is formally equivalent for both the asymmetric and symmetric cases, μ^2 being the subtraction momentum. Then, specifying to the so-called MOM renormalization schemes, which are defined by imposing that all Green's functions take their tree-level values at the subtraction point for a particular choice of momenta configuration, one has for the symmetric case

$$\Delta_R(p^2;p^2) = Z_3^{-1}(p^2)\Delta(p^2) = \frac{1}{p^2}, \tag{2.25}$$

$$T_R^{\text{sym}}(p^2;p^2) = Z_3^{-3/2}(p^2)T^{\text{sym}}(p^2) = \frac{g_R^{\text{sym}}(p^2)}{p^6} \tag{2.26}$$

and for the asymmetric case

$$T_R^{\text{asym}}(p^2;p^2) = Z_3^{-3/2}(p^2)T^{\text{asym}}(p^2) = \Delta_R(0;p^2)\frac{g_R^{\text{asym}}(p^2)}{p^4}. \tag{2.27}$$

Then, Eq. (2.25) yields the renormalization constant Z_3 as a function of the bare propagator, while Eqs. (2.26) and (2.27) provide us with the running coupling defined, respectively, in symmetric and asymmetric MOM schemes,

$$g_R^{\text{sym}}(p^2) = p^3 \frac{T^{\text{sym}}(p^2)}{[\Delta(p^2)]^{3/2}} = p^3 \frac{T_R^{\text{sym}}(p^2,\mu^2)}{[\Delta_R(p^2,\mu^2)]^{3/2}}, \tag{2.28}$$

$$g_R^{\text{asym}}(p^2) = p^3 \frac{T^{\text{asym}}(p^2)}{[\Delta(p^2)]^{1/2}\Delta(0)}$$

$$= p^3 \frac{T_R^{\text{asym}}(p^2;\mu^2)}{[\Delta_R(p^2;\mu^2)]^{1/2}\Delta_R(0;\mu^2)}. \tag{2.29}$$

Both are nonperturbative definitions for the QCD running coupling, that have been extensively studied on the lattice [56–61]. Other MOM schemes based on different QCD vertices and kinematical configurations, as that for the ghost-gluon vertex [62–65], lead to alternative nonperturbative definitions, although all they can be related at any order in perturbation theory [66,67]. Here, in obtaining Eq. (2.28) and Eq. (2.29), we use first Eq. (2.26) and Eq. (2.27), respectively, in order to express the running coupling in terms of bare Green's functions [replacing Z_3 by its Eq. (2.25) bare result] and only then, after realizing that the bare quantities appear as a renormalization-group-independent combination, as they should, replace them by their renormalized counterparts in the far right-hand sides.

In what concerns the 1-PI vertex functions, after applying the renormalization prescription to Eq. (2.12) and Eq. (2.18), respectively, for the symmetric and asymmetric cases, one is left with

$$T_R^{\text{sym}}(p^2;\mu^2) = g_R^{\text{sym}}(\mu^2)\Gamma_{T,R}^{\text{sym}}(p^2;\mu^2)\Delta_R^3(p^2;\mu^2), \tag{2.30}$$

$$T_R^{\text{asym}}(p^2;\mu^2) = g_R^{\text{asym}}(\mu^2)\Gamma_{T,R}^{\text{asym}}(p^2;\mu^2)$$
$$\times \Delta_R(0;\mu^2)\Delta_R^2(p^2;\mu^2), \tag{2.31}$$

where $\Gamma_{T,R}^i(p^2,p^2) = 1$, for i indicating either the symmetric (sym) or the asymmetric (asym) momenta configuration. Then, from either Eq. (2.30) and Eq. (2.28) or Eq. (2.31) and Eq. (2.29), the renormalized 1-PI vertex functions can be calculated for, respectively, the symmetric

and asymmetric momenta configuration and read in both cases

$$g_R^i(\mu^2)\Gamma_{T,R}^i(p^2;\mu^2) = \frac{g_R^i(p^2)}{[p^2\Delta(p^2;\mu^2)]^{3/2}}. \qquad (2.32)$$

This last result is of special interest because it establishes a connection between the three-gluon MOM running coupling,[1] to which many lattice and continuum studies have paid attention, and the vertex function of the amputated three-gluon Green's function, a relevant ingredient within the tower of (truncated) SDEs conceived to address the nonperturbative dynamics of QCD. Both quantities appear related only by the dimensionless gluon propagator dressing function, $D(p^2) = p^2\Delta(p^2)$, which, after the intensive activity developed during the past decade [9–11,15,16,21–23,68–71], is very well understood and accurately known.

III. LATTICE QCD RESULTS

Let us start this section with a reminder of how the three-gluon Green's function is computed from a lattice field theory simulation. For the purpose of a conclusion about qualitative features for its deep infrared behavior, one can simulate lattice volumes in physical units as large as possible but work in the quenched approximation, under the working assumption that light dynamical quarks will only quantitatively affect this behavior. The necessity to focus on the quenched (pure gauge) theory is dictated by the hefty numerical cost imposed by a very large-volume simulation with dynamical fermions. To be more specific, one needs to consider that the most prominent collaborations employ ensembles of gauge fields of which the physical volumes are usually around 3 fm, which is three times smaller than the smallest physical volume that exhibits data points in the deep IR regime where the zero crossing takes place. Sensu stricto, we are concluding here about the zero crossing of the three-gluon Green's function in pure Yang-Mills theory. All the other recent lattice $SU(3)$ investigations [53,54] as well as the previous $SU(2)$ lattice studies [1,2] also worked under the quenched approximation and made conclusions about a theory without light quarks. It cannot be then excluded that the effect of the light quarks might wipe out the zero crossing, as it happens to take place in the far infrared. However, the motivation for the current and past studies in the pure Yang-Mills QCD is two sided: (i) References [40,46–50] claimed that the zero crossing happens as a purely gluodynamical effect, by using the SDE formalism, and then argued it shifts down to deeper momenta by the presence of light

---

[1]Indeed, the quantity that can be generally found in literature is $\alpha(\mu^2) = g^2(\mu^2)/(4\pi)$ which, by squaring the signal of g obtained from the lattice misses the existence of a change of sign, and hence a zero crossing, at very deep IR momentum, for the vertex itself.

quarks [72]. The study of that effect in pure gluodynamics deserves interest *per se* but, if the latter is true, can also provide noteworthy qualitative information about the IR behavior of the QCD gluonic Green's functions. (ii) The mechanism we invoked here to explain the three-gluon sign changing and its zero crossing, as will be discussed in the next section, is the same one, related to the nonperturbative ghost-loop diagram contributing to the gluon self-energy, producing a peak for the gluon propagator at a deep IR nonzero momentum. This gluon propagator peak and the mechanism behind it have been discussed in Ref. [73] within the context of the chiral symmetry restoration in QCD with an increasing number of light flavors. Thus, although our analysis is made in pure gluodynamics, the underlying mechanism for the more apparent feature exhibited by the three-gluon Green's function has, presumably, profound implications in the IR dynamics of QCD.

A noteworthy final remark is that SDE unquenching techniques, as those developed in Refs. [74,75], combined with lattice studies as that of Ref. [7], appear to confirm that the presence of light quarks modifies the ghost and gluon two-point and ghost-gluon three-point Green's functions only slightly at the quantitative level.

A. Generalities

There have been many past lattice studies [57–60,76,77] pursuing mainly the computation of the fundamental QCD parameter, Λ_{QCD}, through a very detailed scrutiny of the running of the three-gluon MOM strong coupling. All these results for the coupling, following Eq. (2.32), can be also used to derive the nonperturbative vertex function, as done in Ref. [53]. Here, apart from taking advantage of them, we aim toward the completion of the preliminary work of Ref. [53], in which we addressed the calculation of the three-gluon vertex function in the four-dimensional $SU(3)$ gauge theory, by simulating QCD on the lattice with the tree-level Symanzik improved gauge action (tlSym) [78] which, in addition to the plaquette term $U_{x,\mu,\nu}^{1\times1}$, also includes rectangular (1×2) Wilson loops $U_{x,\mu,\nu}^{1\times2}$. In particular, the tlSym action reads

$$S_g = \frac{\beta}{3}\sum_x\Bigg\{b_0\sum_{\substack{\mu,\nu=1\\1\leq\mu<\nu}}^{4}[1-\mathrm{ReTr}(U_{x,\mu,\nu}^{1\times1})]$$

$$+ b_1\sum_{\substack{\mu,\nu=1\\\mu\neq\nu}}^{4}[1-\mathrm{ReTr}(U_{x,\mu,\nu}^{1\times2})]\Bigg\}, \qquad (3.1)$$

where $\beta \equiv 6/g_0^2$, g_0 is the bare lattice coupling and one sets $b_1 = -1/12$ and $b_0 = 1-8b_1$ as dictated by the perturbative computation of the improvement coefficient and normalization. The standard Wilson action results from making the choices $b_0 = 1$ and $b_1 = 0$ in Eq. (3.1). As will be seen in the next subsection, we first doubled, in the

present study, the number of gauge-field configurations for the same two lattice setups employed in Ref. [53]; produced then one more ensemble with the tlSym action, defining its lattice setup such as to be left with a physical volume similar to the largest (hence providing reliable estimates for the vertex at equally deep IR momenta) but different lattice spacing; and, finally, obtained three more ensembles of gauge fields simulated with the Wilson action. The idea of including in this detailed analysis an unimproved gauge action originates from our intention of guaranteeing that no issue related to the lattice artifacts from the action discretization is relevant for our purposes. All gauge-field configurations generated by the above actions are gauge fixed to the (minimal) Landau gauge. This is done through the minimization of the following functional [of the $SU(3)$ matrices $U_\mu(x)$],

$$F_U[g] = \text{Re}\left\{\sum_x \sum_\mu \text{Tr}\left[1 - \frac{1}{N}g(x)U_\mu(x)g^\dagger(x+\mu)\right]\right\},$$
(3.2)

with respect to the gauge group element g.

To get as close as possible to the global minimum, we apply a combination of an over-relaxation algorithm and Fourier acceleration, considering the gauge to be fixed when the condition $|\partial_\mu A_\mu|^2 < 10^{-16}$ is fulfilled and the spatial integral of A_0 is constant in time to a relative accuracy better than 10^{-6}. Evidently, this procedure cannot avoid the possibility that lattice Gribov copies are present in the ensemble of gauge fixed configurations. However, extensive studies in the literature of the quenched case (see for example Ref. [5]) show that such copies do not seriously affect the qualitative behavior of the Green's functions in question.

After the lattice configurations have been projected onto the Landau gauge, the gauge field is obtained as

$$A_\mu(x+\hat{\mu}/2) = \frac{U_\mu(x) - U_\mu^\dagger(x)}{2iag_0} - \frac{1}{3}\text{Tr}\frac{U_\mu(x) - U_\mu^\dagger(x)}{2iag_0},$$
(3.3)

with $\hat{\mu}$ indicating the unit lattice vector in the μ direction. It can be then Fourier transformed to momentum space,

$$\tilde{A}_\mu^a(q) = \frac{1}{2}\text{Tr}\sum_x A_\mu(x+\hat{\mu}/2)\exp[iq\cdot(x+\hat{\mu}/2)]\lambda^a,$$
(3.4)

where λ^a are the Gell-Mann matrices and the trace is evaluated in color space, and, finally, the two- and three-point gluon Green's functions are obtained as

$$\Delta_{\mu\nu}^{ab}(p) = \langle\tilde{A}_\mu^a(p)\tilde{A}_\nu^b(-p)\rangle,$$
$$\mathcal{G}_{\mu\nu\rho}^{abc}(p,q,r) = \langle\tilde{A}_\alpha^a(p)\tilde{A}_\mu^b(q)\tilde{A}_\nu^c(r)\rangle,$$
(3.5)

where the $\langle\cdot\rangle$ stands for a Monte Carlo average replacing here the functional integration over the gauge space. Then, as described in the previous section, one can project out the relevant form factors, $T(p^2)$ and $\Delta(p^2)$; renormalize in the MOM scheme; and extract the three-gluon running coupling and the nonperturbative vertex function, following Eqs. (2.28)–(2.32).

To conclude this subsection, we will briefly comment on the role played by the hypercubic artifacts resulting from the lattice discretization and the consequent breaking of the $O(4)$ rotational invariance down to the $H(4)$ isometry group.

The so-called $H(4)$-extrapolation procedure [79–81] has been proven to cure efficiently the lattice data from these artifacts for the two-point gluon and ghost Green's functions, otherwise plaguing their reliable determination. The procedure basically works as follows: any dimensionless correlation function (as $q^2\Delta$ and q^6T) evaluated on the lattice must depend on the (dimensionless) lattice momentum aq_μ, where

$$q_\mu = \frac{2\pi n_\mu}{N_\mu a}, \qquad n_\mu = 0,1,...,N_\mu,$$
(3.6)

N_μ being the number of lattice sites in the μ direction (in our case, $N_\mu = N$ for all μ). Since $O(4)$ is broken down to $H(4)$, it depends not only on a^2q^2 but also on $a^2q^{[4]}/q^2$, at the first order, where $q^{[4]} = \sum_\mu q_\mu^4$ is the first $H(4)$-invariant. All the different configurations of lattice momenta, q_μ, taking the same value for all the $H(4)$-invariants are obviously invariant under $H(4)$ transformations and constitute a so-called $H(4)$-orbit. However, different $H(4)$-orbits may take the same value for q^2, differing only by $q^{[4]}$ or higher-order invariants. Thus, a correlation function evaluated on the lattice at momenta belonging to those different $H(4)$-orbits will differ from each other but must take the same continuum value. This is an apparent manifestation of the $O(4)$-breaking, which the standard recipe to deal with was to introduce a kinematical cut in lattice momenta configuration. The purpose of this kinematical cut was to exclude those momenta carrying a component much larger than the others, only retaining small $a^2q^{[4]}/q^2$ contributions. Subsequently, an average over all the $O(4)$-invariant momenta configurations had to be performed. Instead, in the $H(4)$-extrapolation, one only averages over any combination of momenta within the same $H(4)$-orbit and then extrapolates the results toward the continuum limit where the effect of $a^2q^{[4]}$ vanishes.

An extension of the $H(4)$-extrapolation procedure has also been developed and applied to deal with the hypercubic artifacts of the three-gluon Green's functions in Ref. [61]. Therein, the results obtained from $H(4)$-extrapolation and from the standard $O(4)$-average were compared, and their differences appeared only visible for lattice momenta such

that $\sqrt{a^2q^2} \geq \pi/4$. Here, we have also applied $H(4)$-extrapolation and $O(4)$-average and only retained those lattice momenta which lead to results that compare well after each of the two procedures has been applied.

B. Results

Before displaying the lattice results that we obtained and analyzed in this work, we give first the different lattice setups for all the ensembles produced and exploited here. The simulations parameters are reported in Table I. As can be seen there, we have implemented the two different discretized gauge actions, Wilson and tlSym, described in the previous subsection, adopting three setups for each, corresponding to five different lattice bare couplings (lattice spacings), $g_0^2 = 6/\beta$, their physical volumes ranging from 4.45^4 to 15.6^4 fm^4. For the sake of comparison, we have also exploited the lattice data for the three-gluon running coupling, previously published and analyzed in investigations mostly addressed to the calculation of Λ_{QCD} [57–60,76,77], and derived from them the nonperturbative vertex function. These last data were then obtained from many different lattice simulations, generated with the Wilson gauge action at several β's ranging from 5.6 to 6.0 and physical volumes ranging from 2.4^4 to 5.9^4 fm^4.

Within the approach we follow, the road to the computation of the 1-PI renormalized vertex function implies, in a first step, obtaining the three-gluon running coupling defined in Eqs. (2.28) and (2.29), respectively, for symmetric and asymmetric MOM schemes. This calculation can be directly performed by the implementation of the bare form factors, $\Delta(p^2)$ and $T(p^2)$, projected out from the lattice two- and three-point Green's functions through Eqs. (2.2), (2.13), and (2.16). A main gain of proceeding so is that all the dependence on the cutoff regularization parameters should cancel for the ratios of bare quantities in the definitions of strong coupling and so can be explicitly examined. As far as one properly deals with the lattice discretization artifacts, the outcome of Eqs. (2.28) and (2.29) would only be a function of the squared momentum

at the subtraction point in either the symmetric or the asymmetric configuration, irrespectively of what set of lattice parameters is used. A striking verification of the latter can be seen in the two plots of Fig. 1, where the lattice results for

$$\alpha^i(p^2) = \frac{[g_R^i(p^2)]^2}{4\pi},\tag{3.7}$$

with g_R^i given by Eqs. (2.28) and (2.29), respectively, for $i = \mathrm{sym}$ and $i = \mathrm{asym}$. The strong coupling data obtained from all the lattice ensembles, with very different bare couplings, lattice spacings, and physical volumes, appear to be very well on top of each other when their windows of momenta overlap (where the lattice artifacts happen to be under control). It is worth emphasizing that no renormalization or rescaling factor is needed; the physical scaling shown by the plots of Fig. 1 directly results from the evaluation of Eqs. (2.28) and (2.29) with bare lattice inputs.[2]

Moreover, we have also computed the renormalized three-gluon form factor, T_R^i, following Eq. (2.24), and displayed the results in Fig. 2. For this and, in the following, for all the renormalized quantities, we have chosen $\mu = 4.3$ GeV as the subtraction momentum. Precisely, the use of previously published lattice data together with the new ones produced here made it possible to enlarge the window of momenta for reliable estimates, covering a wider region, containing large UV momenta, where this renormalization point is included. In particular, as it appears indicated by the dashed lines in both panels of Fig. 1, we thus get $\alpha^{\mathrm{asym}}(4.3 \text{ GeV}) = 0.31$, for the symmetric case, and $\alpha^{\mathrm{asym}}(4.3 \text{ GeV}) = 0.27$ for the asymmetric one. The results for the renormalized form factor in the symmetric case robustly show a change of sign and, hence, a zero crossing lying somewhere in between 0.1 and 0.2 GeV. In the asymmetric case, the results are statistically noisier but clearly consistent with the same feature.

Finally, in order to obtain the 1-PI vertex functions, we only need to resort to their connection to the strong coupling, which results in both the symmetric and the asymmetric momenta configurations, from Eq. (2.32). As this equation reads, the calculation involves a gluon two-point Green's function renormalized at the chosen momentum which, precisely, carries all the renormalization-point dependence for the vertex function. This two-point Green's function being a renormalized quantity, on the understanding of which exists now a clear consensus and which appears to be very accurately known, we can take for it the results obtained with the best available gluon propagator lattice data in the literature, namely, those simulated with the largest physical volume [5]. We thus only need to

TABLE I. Lattice setup parameters for the simulations employed here using either the Wilson or tlSym discretized gauge actions. The lattice bare coupling, for the case of $SU(3)$, is given by $g_0^2 = 6/\beta$, N stands for the number of lattice sites in any of the four dimensions, and the physical volume is obtained from the lattice spacings taken from Refs. [82] for the Wilson action and Ref. [83] for tlSym. The number of the exploited configurations of gauge fields is also given in the fourth row.

β	4.2	3.8	3.9	5.8	5.6	5.6
N	32	48	64	48	48	52
(Volume)$^{1/4}$ [fm]	4.45	13.7	15.6	6.72	11.3	12.3
Configurations	420	1050	2000	960	1920	1790
Action	tlSym	tlSym	tlSym	Wilson	Wilson	Wilson

---

[2]No direct rescaling is needed for the coupling; however, we have corrected by 5%—admitting that relative error—the value of the lattice spacing in physical units for the Wilson-action setup at $\beta = 5.8$, with the criterion of obtaining an optimal scaling.
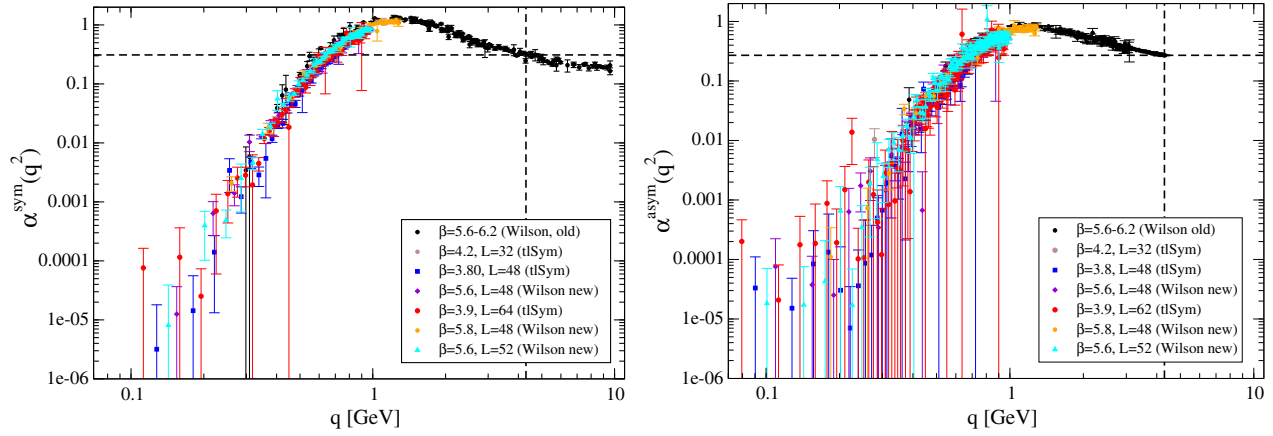
FIG. 1. The strong running coupling, Eq. (3.7), in both symmetric (left panel) and asymmetric (right panel) MOM schemes, where g_R is computed by using, respectively, Eqs. (2.28) and (2.29). We use logarithmic scales for both axes in both panels. Data obtained from the six setups reported in Table I appear displayed with different symbols and colors (as shown in the legends), and, additionally, data previously published and investigated in Refs. [57–60,76,77] are plotted (black solid circles), for the sake of comparison and to cover the UV region where we estimate $\alpha^{\text{sym}}(4.3 \text{ GeV}) = 0.31$ and $\alpha^{\text{asym}}(4.3 \text{ GeV}) = 0.27$ (dashed lines).
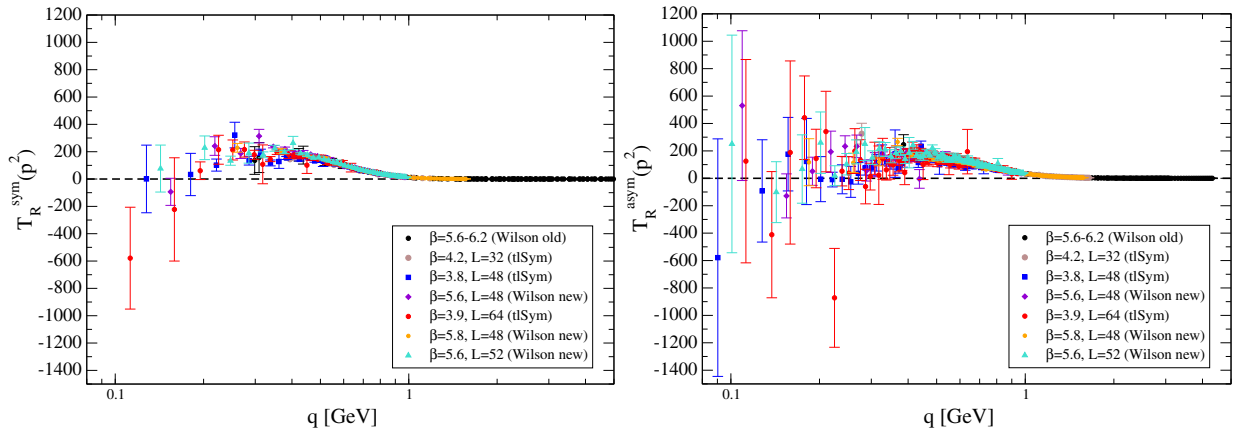
FIG. 2. The three-gluon form factor, renormalized at $\mu = 4.3$ GeV according to Eq. (2.24), after being projected out through Eqs. (2.13) and (2.16) from, respectively, the symmetric (left panel) and asymmetric (right panel) lattice bare Green's functions.

combine, according to Eq. (2.32), the renormalized results for the two-point function with those for the three-gluon strong coupling, shown in Fig. 1, directly obtained from bare lattice Green's functions. Or one can apply instead Eqs. (2.30) and (2.31) and use there the results for the renormalized three-gluon form factors collected in Fig. 2. In both cases, we will be left with the results for the 1-PI vertex functions, which appear displayed in Fig. 3.

In Fig. 3, we have grouped only the results obtained with the same gauge action, either Wilson (upper panels) or tlSym (lower panels). In both cases, the zero-crossing feature clearly happens for the symmetric momenta configuration (left) and is remarkably consistent with the (noisier) asymmetric configuration (right). Indeed, the Wilson-action symmetric-configuration data also appear to offer a robust confirmation for the happening of the zero

crossing.[3] With the aim of guiding the eye for comparative purposes, we have also included, in all the plots, the SDE-inspired fits that will be further discussed in the next section. It is not worthless to emphasize that, even if one is willing to analyze independently any of the four lattice setups producing estimates for momenta lying on the zero-crossing region ($\beta = 5.6$ for 48^4 and 52^4 lattices, in the Wilson case, and $\beta = 3.8$ and $\beta = 3.9$, for tlSym), the attained conclusions would be plainly compatible with a global analysis, as the data from any of these setups appear to be consistent with each other and behave as expected, if the SDE interpretation for the zero crossing is correct.

---

[3]This is in agreement with the very recent claim for further evidences for the zero crossing in the asymmetric three-gluon vertex [54].
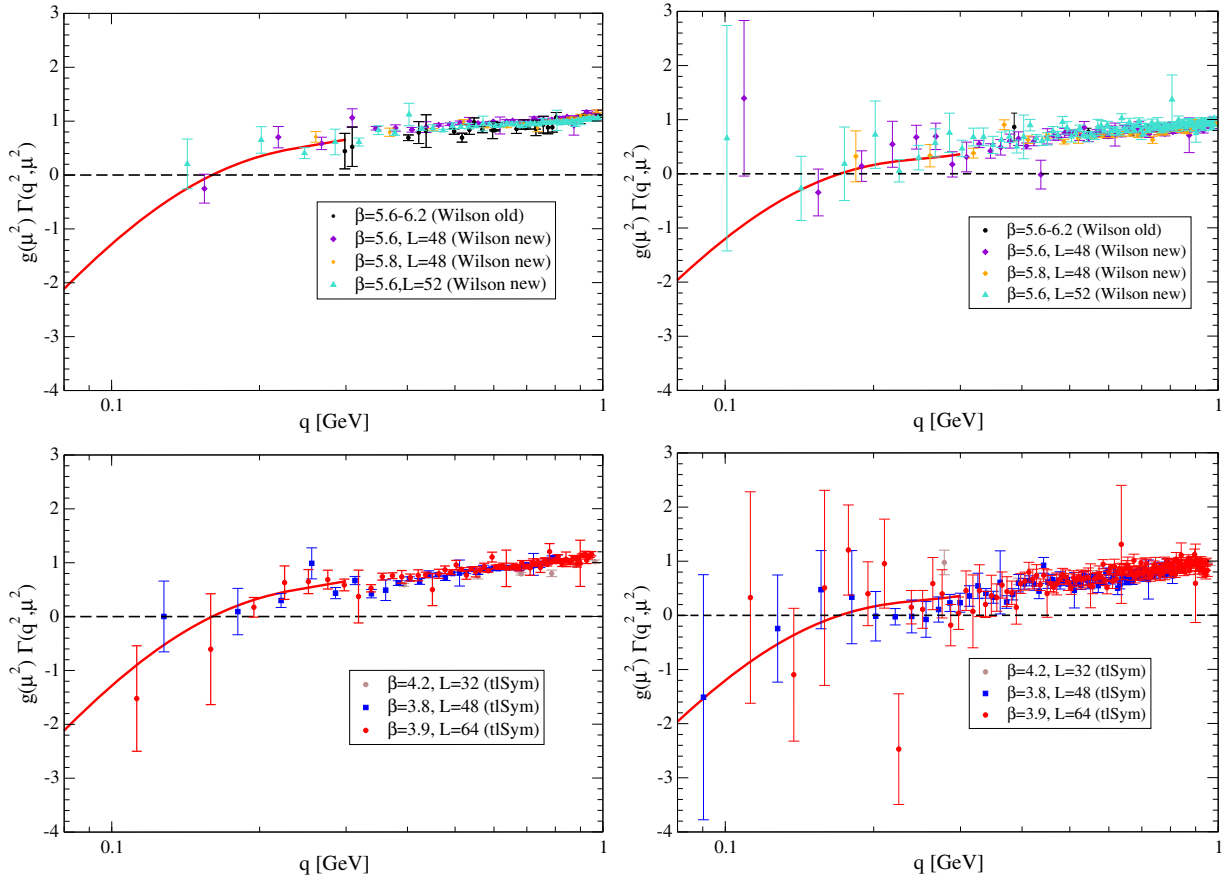
FIG. 3.   Three-gluon 1-PI form factors obtained from lattice results simulated with the Wilson (upper panels) and the tlSym (lower panels) gauge actions, plotted in terms of the momenta displayed in logarithmic scale, for symmetric (left) and asymmetric (right) momenta configuration. The renormalization point is $\mu = 4.3$ GeV. The red solid lines result from SDE-based fits which will be explained in the next section and which are included here for comparative purposes.

IV. SDE-BASED ANALYSIS

As was preliminarily shown in Ref. [53], lattice data for the three-gluon 1-PI vertex functions, in particular the change of sign and the zero crossing they exhibit in the deep IR, appear to be consistent with a noteworthy effect that had been previously shown in literature (notably in Refs. [40,46]), namely, the (four-dimensional) logarithmic singularity induced in the three-gluon vertex function by the *nonperturbative* ghost-loop diagram contributing to the gluon propagator SDE. Specifically, employing a nonperturbative ansatz for the ghost-gluon vertex that satisfies the appropriate STI, one is left with the following IR contribution to the gluon self-energy for this ghost-loop diagram [46],

$$\Pi_c(p^2) = \frac{g^2 C_A}{6} p^2 F(p^2) \int_k \frac{k^2}{k^2(k+p)^2}, \quad (4.1)$$

where C_A is the Casimir eigenvalue in the adjoint representation, $F(p^2)$ is the ghost dressing function, and $\int_k \equiv \mu^\varepsilon/(2\pi)^d \int d^d k$ is the dimensional regularization measure with $d = 4 - \varepsilon$, and μ is the 't Hooft mass. The above leading contribution in the vanishing momentum limit,

$p^2 \to 0$, evidently behaves like $p^2 \ln p^2/\mu^2$ and leads to the following very accurate parametrization,

$$\Delta_R^{-1}(p^2; \mu^2) \underset{p^2/\mu^2 \ll 1}{=} p^2 \left[a + b \ln \frac{p^2 + m^2}{\mu^2} + c \ln \frac{p^2}{\mu^2} \right] + m^2,$$

$$(4.2)$$

for the IR form of the gluon propagator which emerges from its complete SDE, with a, b, c, and m^2 suitable renormalization-dependent parameters capturing explicitly both the effect of the ghost loop sketched by Eq. (4.1) and the finiteness of the gluon propagator at vanishing momentum, $\Delta_R^{-1}(0; \mu^2) = m^2$. Note that this finiteness is the consequence of an effective mass being acquired which *protects* the gluon loops against the logarithmic singularities resulting from the ghost loops.[4]

---

[4]Then, although the ghost is directly transparent to the mass-generation mechanism, the absence of additional singularities resulting from the nonperturbative gluon loops, which owes to the gluon mass generation, guarantees the finiteness of the ghost dressing function at vanishing momentum.

Any standard Green's function can be related to the same one with *background* legs, within the PT-BFM approach, by the use of the so-called *background quantum* identities [41,84,85]). The ones with background legs, when projected according to Eqs. (2.13) and (2.16) and by virtue of the Abelian STI that the PT-BFM propagators are constructed to obey, will be led in the IR by the derivative of the inverse of the gluon propagator, represented by Eq. (4.2) [46]. Thus, the three-gluon 1-PI form factors derived from the background Green's functions can be proven to behave in the deep IR as

$$\Gamma_{T,R}^{i,(B)}(p^2;\mu^2) \underset{p^2/\mu^2 \ll 1}{\simeq} F_R(0;\mu^2) \frac{\partial}{\partial p^2} \Delta_R^{-1}(p^2;\mu^2) + \cdots$$

$$\simeq F_R(0;\mu^2)\left(a + b\ln\frac{m^2}{\mu^2} + c\right)$$

$$+ cF_R(0;\mu^2)\ln\frac{p^2}{\mu^2} + \cdots, \quad (4.3)$$

where $F_R(0;\mu^2)$ is the renormalized ghost dressing function evaluated at zero momentum and where the dots stand for subleading corrections that, as discussed in Ref. [83], might be collectively taken into account by adding an extra constant term which, contrarily to the leading contribution, depends *a priori* on the momenta configuration. On the other hand, the connection between the background and the standard vertex functions is controlled by the ghost-gluon dynamics and will essentially introduce a finite correction not modifying the leading logarithmic divergence in Eq. (4.3). Thus, we can eventually write

$$g_R^i(\mu^2)\Gamma_R^i(p^2;\mu^2) = a_{\ln}^i(\mu^2)\ln\frac{p^2}{\mu^2} + a_0^i(\mu^2) + o(1), \quad (4.4)$$

where $a_0^i(\mu^2)$ is a constant which borrows from all the subleading corrections and which will be considered, in the following, as a free parameter to be fitted, while the

logarithmic slope, $a_{\ln}^i(\mu^2) = g_R^i(\mu^2)cF_R(0;\mu^2)$, is known from gluon and ghost two-point Green's functions and from the value of the three-gluon coupling at the renormalization point. Indeed, at $\mu = 4.3$ GeV, we have $F_R(0,\mu) \simeq 2.9$ from Ref. [5] and $c \in (0.35, 0.55)$ from Ref. [83] (where the range is thought to account for the uncertainty coming from the two fits of Eq. (4.2) to data from 80^4 and 96^4 lattices at $\beta = 5.7$ [5]) and have estimated the coupling from the data displayed in Fig. 1 for both symmetric and asymmetric configurations. We thus obtain the values for $a_{\ln}^i$ reported in Table II (first or second column for the symmetric case and fourth or fifth for the asymmetric case) and used in Fig. 4.

However, Eq. (4.4), with values for $a_{\ln}^i$ lying inside its predicted range, can hardly account for data within a fitting window of momenta up to 0.2 GeV, in particular for the symmetric case (see the brown band in the left plot of Fig. 4). Otherwise said, a fit of Eq. (4.4) with both a_0^i and $a_{\ln}^i$ as free parameters would yield an optimal best-fit result for the latter about twice smaller than the lowest value reported in Table II. This seems to suggest that the first subleading correction, at least, is needed to describe properly the data around 0.2 GeV. As we know from Refs. [73,86,87], the first subleading correction introduced by the ghost-gluon dynamics should behave as $p^2\ln(p^2)$. We thus correct Eq. (4.4) as

$$g_R^i(\mu^2)\Gamma_R^i(p^2;\mu^2) = a_{\ln}^i(\mu^2)\ln\frac{p^2}{\mu^2} + a_0^i(\mu^2)$$

$$+ a_2^i(\mu^2)p^2\ln\frac{p^2}{M^2} + o(p^2), \quad (4.5)$$

where, again, a_2^i and M will be free parameters capturing subleading contributions. M differs *a priori* from the renormalization point since it is absorbing the $\mathcal{O}(p^2)$-contribution which, for the sake of consistence, is also required. Then, by applying Eq. (4.5) with $a_{\ln}^i$ also as a free

TABLE II. Best-fit parameters obtained by applying the SDE-based ansatz to describe the three-gluon 1-PI form factors in symmetric and asymmetric configurations. The first and fourth columns correspond to fits of Eq. (4.4) to, respectively, symmetric and asymmetric lattice data, with $a_{\ln}^i$ fixed by the estimates (lower and upper bounds) of c in Ref. [83]; the second and fifth stand for the fits with Eq. (4.5), also with $a_{\ln}^i$ fixed in the same way; the third stands for a fit to the symmetric data with Eq. (4.5) and all the parameters free; the sixth results from taking the value of c derived from symmetric data and so fixing $a_{\ln}^{\text{asym}}$ in a fit of Eq. (4.5) to the asymmetric data. The asterisk indicates that numbers do not result from a fit but are imposed, as above explained. The renormalization point is $\mu = 4.3$ GeV.

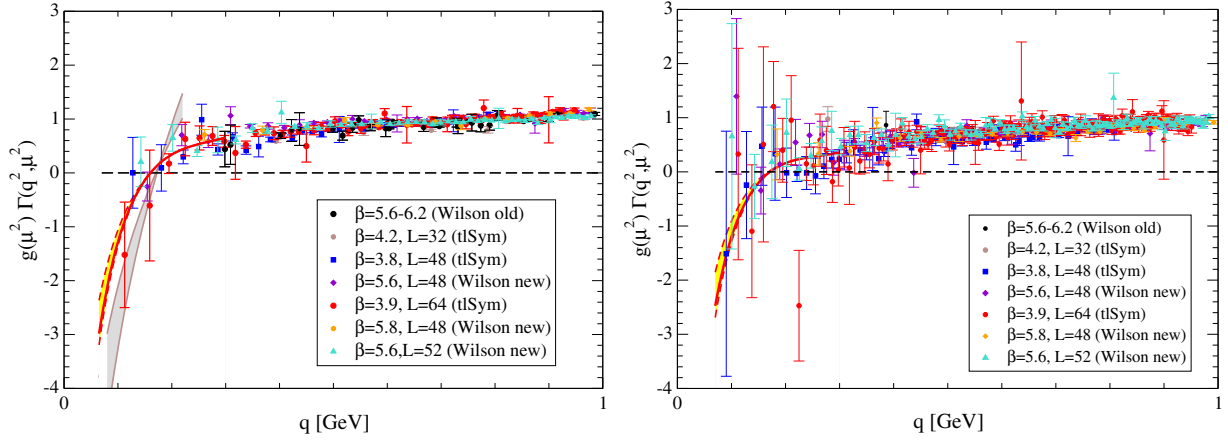| | $i = \text{sym}$ | | | $i = \text{asym}$ | | |
	Eq. (4.4)	Eq. (4.5)	Eq. (4.5)	Eq. (4.4)	Eq. (4.5)	Eq. (4.5)
$a_0^{(i)}$	13.2–20.0	15.3–23.7	20.6	12.4–18.8	14.5–22.3	19.5
$a_{\ln}^{(i)}$	2.05–3.12(*)	2.05–3.12(*)	2.74	1.92–2.91(*)	1.92–2.91(*)	2.55(*)
$a_2^{(i)}$	...	21.3–41.7	34.4	...	26.1–42.5	36.6
M [GeV]	...	0.78–0.71	0.72	...	0.70–0.69	0.69

FIG. 4.   The same three-gluon 1-PI form factors displayed in Ref. 3, plotted now all together and making use of a linear scale, for the symmetric (left) and asymmetric (right) momenta configurations. The renormalization point is $\mu = 4.3$ GeV. The red solid and dashed lines result from the best fits with Eq. (4.5), while the brown solid lines correspond to Eq. (4.4), as explained in the text. Yellow and brown bands depict the uncertainty resulting from the range of c estimated in Ref. [83], in the cases of, respectively, Eq. (4.5)'s and Eq. (4.4)'s fits.

parameter, we get the best fits displayed in the solid red lines in the left panels (for the symmetric case) of Figs. 3 and 4. These fits give a nice description of all data below 0.3 GeV and correspond to the best-fit parameters reported in Table II (third column). In particular, the optimal value for $a_{\ln}^{\rm sym}(\mu^2)$, combined with $F_R(0, \mu^2)$ and $g_R^{\rm sym}(\mu^2)$, allows for a prediction of the coefficient c controlling the massless ghost-loop contribution,

$$c \simeq 0.48, \qquad (4.6)$$

which happens to agree pretty well with the range of results obtained in Ref. [53] from gluon propagator lattice data given in Ref. [5], namely, $c \in (0.35, 0.55)$. Next, we can take this best-fit estimate of c, obtained from the symmetric configuration to determine $a_{\ln}^{\rm asym}$, apply it in Eq. (4.5), and produce then the best fits for the asymmetric configuration displayed in the right panels of Figs. 3 and 4. In the view of all the plots and, specially, of Eq. (4.6), it can be concluded that the lattice three-gluon vertex data we produced and introduced in the previous section (part of which were published and analyzed in Ref. [53]) are plainly consistent with their SDE description based on the PT-BFM approach and with the lattice ghost and gluon two-point Green's functions. We have also made fits with $a_{\ln}^{(i)}$ fixed by the upper and lower bounds for the range of c given in Ref. [53] and produced the red dotted lines in the plots. The yellow band in between depicts, precisely, the region where the SDE-based ansatz fits optimally the data, in consistence with the lattice two-point Green's functions.

The position of the zero crossing depends on the competition of the logarithm coming from the ghost loop, controlled by the coefficient c, against the effect of the finite subleading corrections, the details of which we only

precise here by a direct fit to three-gluon lattice data. Applying the best fit of Eq. (4.5) to the lattice data, the zero crossing is found to lie on $p_0^{\rm sym} \simeq 0.17$ GeV, for the symmetric case, and $p_0^{\rm asym} \simeq 0.16$ GeV, for the asymmetric case, while, had we employed Eq. (4.4) with the best-fit parameters of Table II, one would have obtained $p_0^i \simeq 0.17$ GeV, for both the symmetric and the asymmetric cases. Of course, there are non-negligible statistic and systematic uncertainties for these results. For instance, we estimate a relative error of around 15% for the position of the zero crossing, when using Eq. (4.4) in the symmetric case, while, in the much noisier asymmetric case, we get a relative error of 34%. Both are just statistical errors. In this work, we do not aim for a very precise determination of the zero crossing but for a very strong confirmation that, after the appropriate projection, the nonperturbative ghost-loop contribution induces a logarithmic singularity at vanishing momentum for the three-gluon form factors—independently of which particular momenta configuration we are considering—which drives the vertex under question from positive to negative values.

V. CONCLUSIONS

We have investigated further the IR structure of the three-gluon vertex, especially by studying the nonperturbative form factor associated to the tree-level tensor, precisely the one that should be invoked in the definition of the running strong coupling under the MOM renormalization prescription. Previous studies, both in lattice and continuous QCD—following various distinct approaches—have provided evidence for a change of sign of this form factor at a given momentum lying in the deep IR domain, at least for QCD without light quarks. It has been argued that the effect of light quarks would be only quantitative and consists of

the shifting of the corresponding "zero crossing" down to the IR. However, the issue has not been completely settled, and one should be cautious about concluding the appearance of a zero crossing in realistic QCD.

In this work, still exploiting gauge-field configurations from quenched lattice QCD simulations but at very large physical volumes, we presented a more refined and elaborated analysis of the detection of the zero crossing for some three-gluon vertex form factors. This very specific infrared feature is posited to be closely related to the masslessness of the Faddeev-Popov ghost propagator circulating in the nonperturbative loop diagrams contributing to the gluon vacuum polarization, which is the underlying source of the negative singularity for the three-gluon form factors forcing the change of sign. Indeed, such a negative singularity is more striking and easily discernible as an effect of the nonperturbative ghost loop than its direct impact on the gluon propagator. Provided that the nonperturbative ghost loops have been also recently shown to have a noteworthy impact on the quark-gluon interaction kernel and, hence, on a process-independent effective strong coupling based on the PT-BFM approach [88], the confirmation of the zero crossing and the numerical estimate of the ghost-loop impact [expressed by the coefficient c in Eq. (4.2)] are also interesting results with possible phenomenological implications.

Compared to previous studies of the topic, we provided here more and stronger corroborative evidence to the statement in question. In particular, by pushing the statistics and by employing different lattice actions (Wilson plaquette and tree-level Symanzik improved), we have under much tighter control statistical and systematical uncertainties which lead us to make more clear statements about both the symmetric as well as the asymmetric momentum configurations. We provided a fully comprehensive and refined analysis grounded on its understanding within the framework of SDE under the PT-BFM scheme and recapitulated the basic argument on how, within this approach, the nonperturbative ghost-loop diagrams can lead to such a remarkable effect. On the basis of both our employment of pure gauge simulations with large physical volumes and our refined analysis, we managed to further solidify the zero crossing not only of the symmetric kinematical setup but also of the much noisier asymmetric one that was previously smudged due to high statistical fluctuations.

ACKNOWLEDGMENTS

[1] A. Cucchieri, A. Maas, and T. Mendes, Phys. Rev. D **74**, 014503 (2006).

[2] A. Cucchieri, A. Maas, and T. Mendes, Phys. Rev. D **77**, 094510 (2008).

[3] A. Cucchieri and T. Mendes, Proc. LAT2007 (**2007**), 297.

[4] A. Cucchieri and T. Mendes, Proc. Sci. QCD-TNT09 (**2009**) 026.

[5] I. Bogolubsky, E. Ilgenfritz, M. Muller-Preussker, and A. Sternbeck, Phys. Lett. B **676**, 69 (2009).

[6] O. Oliveira and P. Silva, Proc. Sci. LAT2009 (**2009**) 226.

[7] A. Ayala, A. Bashir, D. Binosi, M. Cristoforetti, and J. Rodriguez-Quintero, Phys. Rev. D **86**, 074512 (2012).

[8] A. G. Duarte, O. Oliveira, and P. J. Silva, Phys. Rev. D **94**, 014502 (2016).

[9] A. C. Aguilar, D. Binosi, and J. Papavassiliou, Phys. Rev. D **78**, 025010 (2008).

[10] Ph. Boucaud, J. P. Leroy, A. Le Yaouanc, J. Micheli, O. Pène, and J. Rodríguez-Quintero, J. High Energy Phys. 06 (2008) 099.

[11] C. S. Fischer, A. Maas, and J. M. Pawlowski, Ann. Phys. (Amsterdam) **324**, 2408 (2009).

[12] J. Rodriguez-Quintero, J. High Energy Phys. 01 (2011) 105.

[13] M. R. Pennington and D. J. Wilson, Phys. Rev. D **84**, 119901 (2011).

[14] P. Maris and C. D. Roberts, Int. J. Mod. Phys. E **12**, 297 (2003).

[15] A. Aguilar and A. Natale, J. High Energy Phys. 08 (2004) 057; erratum added online, 2005, arXiv:hep-ph/0408254.

[16] P. Boucaud *et al.*, arXiv:hep-ph/0507104.

[17] C. S. Fischer, J. Phys. G **32**, R253 (2006).

[18] K.-I. Kondo, Phys. Rev. D **74**, 125003 (2006).

[19] D. Binosi and J. Papavassiliou, Phys. Rev. D **77**, 061702 (2008).

[20] D. Binosi and J. Papavassiliou, J. High Energy Phys. 11 (2008) 063.

[21] Ph. Boucaud, J. P. Leroy, A. Le Yaouanc, J. Micheli, O. Pène, A. Y. Lokhov, C. Roiesnel, and J. Rodríguez-Quintero, J. High Energy Phys. 03 (2007) 076.

[22] D. Dudal, S. Sorella, N. Vandersickel, and H. Verschelde, Phys. Rev. D **77**, 071501 (2008).

[23] D. Dudal, J. A. Gracey, S. P. Sorella, N. Vandersickel, and H. Verschelde, Phys. Rev. D **78**, 065047 (2008).

[24] K.-I. Kondo, Phys. Rev. D **84**, 061702 (2011).

[25] A. P. Szczepaniak and E. S. Swanson, Phys. Rev. D **65**, 025012 (2001).

[26] A. P. Szczepaniak, Phys. Rev. D **69**, 074031 (2004).

[27] D. Epple, H. Reinhardt, W. Schleifenbaum, and A. Szczepaniak, Phys. Rev. D **77**, 085007 (2008).

[28] A. P. Szczepaniak and H. H. Matevosyan, Phys. Rev. D **81**, 094007 (2010).

[29] P. Watson and H. Reinhardt, Phys. Rev. D **82**, 125010 (2010).

[30] P. Watson and H. Reinhardt, Phys. Rev. D **85**, 025014 (2012).

[31] L. Chang and C. D. Roberts, Phys. Rev. Lett. **103**, 081601 (2009).

[32] L. Chang, C. D. Roberts, and P. C. Tandy, Chin. J. Phys. **49**, 955 (2011).

[33] S.-x. Qin, L. Chang, Y.-x. Liu, C. D. Roberts, and D. J. Wilson, Phys. Rev. C **84**, 042202 (2011).

[34] S.-x. Qin, L. Chang, Y.-x. Liu, C. D. Roberts, and D. J. Wilson, Phys. Rev. C **85**, 035202 (2012).

[35] A. Bashir, L. Chang, I. C. Cloet, B. El-Bennich, Y.-X. Liu, C. D. Roberts, and P. C. Tandy, Commun. Theor. Phys. **58**, 79 (2012).

[36] G. Eichmann, Prog. Part. Nucl. Phys. **67**, 234 (2012).

[37] I. C. Cloet and C. D. Roberts, Prog. Part. Nucl. Phys. **77**, 1 (2014).

[38] D. Binosi, L. Chang, J. Papavassiliou, and C. D. Roberts, Phys. Lett. B **742**, 183 (2015).

[39] M. Tissier and N. Wschebor, Phys. Rev. D **82**, 101701 (2010).

[40] M. Tissier and N. Wschebor, Phys. Rev. D **84**, 045018 (2011).

[41] D. Binosi and J. Papavassiliou, Phys. Rep. **479**, 1 (2009).

[42] J. M. Cornwall, Phys. Rev. D **26**, 1453 (1982).

[43] C. W. Bernard, Nucl. Phys. **B219**, 341 (1983).

[44] J. F. Donoghue, Phys. Rev. D **29**, 2559 (1984).

[45] O. Philipsen, Nucl. Phys. **B628**, 167 (2002).

[46] A. C. Aguilar, D. Binosi, D. Ibaez, and J. Papavassiliou, Phys. Rev. D **89**, 085008 (2014).

[47] M. Pelaez, M. Tissier, and N. Wschebor, Phys. Rev. D **88**, 125003 (2013).

[48] A. Blum, M. Q. Huber, M. Mitter, and L. von Smekal, Phys. Rev. D **89**, 061703 (2014).

[49] G. Eichmann, R. Williams, R. Alkofer, and M. Vujinovic, Phys. Rev. D **89**, 105014 (2014).

[50] A. K. Cyrol, L. Fister, M. Mitter, J. M. Pawlowski, and N. Strodthoff, Phys. Rev. D **94**, 054005 (2016).

[51] D. Binosi, D. Ibaez, and J. Papavassiliou, J. High Energy Phys. 09 (2014) 059.

[52] A. K. Cyrol, M. Q. Huber, and L. von Smekal, Eur. Phys. J. C **75**, 102 (2015).

[53] A. Athenodorou, D. Binosi, P. Boucaud, F. De Soto, J. Papavassiliou, J. Rodriguez-Quintero, and S. Zafeiropoulos, Phys. Lett. B **761**, 444 (2016).

[54] A. G. Duarte, O. Oliveira, and P. J. Silva, Phys. Rev. D **94**, 074502 (2016).

[55] J. S. Ball and T.-W. Chiu, Phys. Rev. D **22**, 2550 (1980).

[56] B. Allés, D. S. Henty, H. Panagopoulos, C. Parrinello, C. Pittori, and D. G. Richards, Nucl. Phys. **B502**, 325 (1997).

[57] P. Boucaud, J. Leroy, J. Micheli, O. Pène, and C. Roiesnel, J. High Energy Phys. 10 (1998) 017.

[58] P. Boucaud, A. Le Yaouanc, J. Leroy, J. Micheli, O. Pène, and J. Rodríguez-Quintero, Phys. Lett. B **493**, 315 (2000).

[59] P. Boucaud, A. Le Yaouanc, J. Leroy, J. Micheli, O. Pène, and J. Rodríguez-Quintero, Phys. Rev. D **63**, 114003 (2001).

[60] F. De Soto and J. Rodriguez-Quintero, Phys. Rev. D **64**, 114003 (2001).

[61] P. Boucaud, M. Brinet, F. De Soto, V. Morenas, O. Pne, K. Petrov, and J. Rodriguez-Quintero, J. High Energy Phys. 04 (2014) 086.

[62] L. von Smekal, R. Alkofer, and A. Hauck, Phys. Rev. Lett. **79**, 3591 (1997).

[63] A. Sternbeck *et al.*, Proc. Sci. LAT2007 (**2007**) 256.

[64] P. Boucaud, F. De Soto, J. Leroy, A. Le Yaouanc, J. Micheli, O. Pène, and J. Rodríguez-Quintero, Phys. Rev. D **79**, 014508 (2009).

[65] L. von Smekal, K. Maltman, and A. Sternbeck, Phys. Lett. B **681**, 336 (2009).

[66] K. G. Chetyrkin and T. Seidensticker, Phys. Lett. B **495**, 74 (2000).

[67] K. Chetyrkin and A. Retey, arXiv:hep-ph/0007088.

[68] A. C. Aguilar and J. Papavassiliou, J. High Energy Phys. 12 (2006) 012.

[69] A. C. Aguilar, D. Binosi, J. Papavassiliou, and J. Rodriguez-Quintero, Phys. Rev. D **80**, 085018 (2009).

[70] C. S. Fischer and J. M. Pawlowski, Phys. Rev. D **80**, 025023 (2009).

[71] A. Aguilar, D. Binosi, and J. Papavassiliou, J. High Energy Phys. 07 (2010) 002.

[72] R. Williams, C. S. Fischer, and W. Heupel, Phys. Rev. D **93**, 034026 (2016).

[73] D. Binosi, C. D. Roberts, and J. Rodriguez-Quintero, arXiv:1611.03523.

[74] A. C. Aguilar, D. Binosi, and J. Papavassiliou, Phys. Rev. D **86**, 014032 (2012).

[75] A. C. Aguilar, D. Binosi, and J. Papavassiliou, Phys. Rev. D **88**, 074010 (2013).

[76] P. Boucaud, F. De Soto, A. Le Yaouanc, J.P. Leroy, J. Micheli, H. Moutarde, O. Pene, and J. Rodriguez-Quintero, J. High Energy Phys. 04 (2003) 005.

[77] P. Boucaud, F. De Soto, A. Le Yaouanc, J.P. Leroy, J. Micheli, O. Pene, and J. Rodriguez-Quintero, Phys. Rev. D **70**, 114503 (2004).

[78] P. Weisz, Nucl. Phys. **B212**, 1 (1983).

[79] D. Becirevic, P. Boucaud, J. Leroy, J. Micheli, O. Pene, J. Rodriguez-Quintero, and C. Roiesnel, Phys. Rev. D **60**, 094509 (1999).

[80] D. Becirevic, P. Boucaud, J. Leroy, J. Micheli, O. Pene, J. Rodriguez-Quintero, and C. Roiesnel, Phys. Rev. D **61**, 114508 (2000).

[81] F. de Soto and C. Roiesnel, J. High Energy Phys. 09 (2007) 007.

[82] M. Guagnelli, R. Petronzio, J. Rolf, S. Sint, R. Sommer, and U. Wolff (ALPHA Collaboration), Nucl. Phys. **B595**, 44 (2001).

[83] A. Athenodorou, P. Boucaud, F. De Soto, J. Rodrguez-Quintero, and S. Zafeiropoulos, Phys. Lett. B **760**, 354 (2016).

[84] P. A. Grassi, T. Hurth, and M. Steinhauser, Ann. Phys. (N.Y.) **288**, 197 (2001).

[85] D. Binosi and J. Papavassiliou, Phys. Rev. D **66**, 111901 (2002).

[86] Ph. Boucaud, M. E. Gómez, J. P. Leroy, A. Le Yaouanc, J. Micheli, O. Pène, and J. Rodríguez-Quintero, Phys. Rev. D **82**, 054007 (2010).

[87] J. Rodriguez-Quintero, Phys. Rev. D **83**, 097501 (2011).

[88] D. Binosi, C. Mezrag, J. Papavassiliou, C. D. Roberts, and J. Rodriguez-Quintero, arXiv:1612.04835.